HOSTED BY

ELSEVIER

Available online at www.sciencedirect.com

ScienceDirect

journal homepage: www.elsevier.com/locate/ajps

Original Research Paper

Effects of particle size on the triboelectrification phenomenon in pharmaceutical excipients: Experiments and multi-scale modeling

Raj Mukherjee [a,1], *Vipul Gupta* [a,1], *Shivangi Naik* [a], *Saurabh Sarkar* [a], *Vinit Sharma* [b], *Prasad Peri* [c], *Bodhisattwa Chaudhuri* [a,b,*]

[a] *Department of Pharmaceutical Sciences, University of Connecticut, Storrs, CT 06269, USA*
[b] *Institute of Material Sciences, University of Connecticut, Storrs, CT 06269, USA*
[c] *Merck Sharp and Dohme, West Point, PA 19486, USA*

ARTICLE INFO

Article history:
Received 1 April 2016
Accepted 18 April 2016
Available online 10 May 2016

Keywords:
Tribocharging
Work function
Excipient
Discrete Element Modeling

ABSTRACT

Particle sizes play a major role to mediate charge transfer, both between identical and different material surfaces. The study probes into the probable mechanism that actuates opposite polarities between two different size fractions of the same material by analyzing the charge transfer patterns of two different sizes of microcrystalline cellulose (MCC). Quantum scale calculations confirmed alteration of charge transfer capacities due to variation of moisture content predicted by multiple surface and bulk analytical techniques. Discrete Element Method (DEM) based multi-scale computational models pertinent to predict charge transfer capacities were further implemented, and the results were in accordance to the experimental charge profiles.

1. Introduction

Tribocharging refers to the phenomenon of charging two solid surfaces when they are brought into contact and separated [1,2], acquiring positive or negative polarities based on the mechanisms of charge transfer. The hazards and problems related to tribocharging have been long known, and reports of related instances can be dated back to as early as 1745, when jets of water from an electrostatic machine led to the ignition of Spritius Frobenii (a sulfuric ether) [3,4]. Among multiple incidents reported in the past century include severe explosions

* *Corresponding author.* Department of Pharmaceutical Sciences, University of Connecticut, Storrs, CT 06269, USA. Tel.: +1 (860) 486 4861; fax: +1 (860) 486 2076.
E-mail address: bodhi.chaudhuri@uconn.edu (B. Chaudhuri).

[1] Shared first authorship.

Abbreviations: φ, Work Function; ε_o, permittivity of the free space; ε, Relative permittivity of the medium; eV, electron Volts; E_{gap}, Energy gap between HOMO and LUMO; F_c, Columbic Force; F_N, Normal Forces; F_{sc}, Screened Columbic Force; F_T, Tangential Forces; ΣF_i, Net force acting on a particle; IP, Ionization Potential; K_B, Boltzmann's constant; m_i, Mass of the particle; n_i, number of particles within the screening distance; q, Charge of particle; q_e, Charge of an electron; s, Contact area; T, Temperature in Kelvin; ΣT_i, Net torque acting on the particle; z, Cut off distance for charge transfer.

http://dx.doi.org/10.1016/j.ajps.2016.04.006

in 1969 that took place when 200,000 ton oil tankers exploded while washing with high velocity water jets [5]. Repeated accidents during the period 1950–1970 in different industries including petroleum [6], defense, chemical [6] and powder handling triggered meticulous investigation of the underlying cause of these incidents (i.e. tribocharging). Since then more than several thousands of research articles have been published discussing tribocharging in various fields ranging from pharmaceuticals, explosives, xerography, food, polymers, nutraceuticals, catalysts, etc.

Tribocharging triggers multiple impediments in industrial storage and handling [7,8], including jamming [9], segregation [10], loss of material due to adhesion, reduced fill, change in dispersion or aggregation behavior in fluidized beds, pneumatic conveying [11], functional interruptions of equipment components, in drug delivery devices such as dry powder inhalers [12,13] and often personal discomforts due to electric shock. Tribocharging can also lead to potential hazards of fire explosions by the discharge of static charges (known as charge relaxation) from the tribocharged surfaces in the presence of low flash point solvents such as ethanol. Flash point of 70% ethanol is 16.6 °C, which means that even at a temperature as low as 16.6 °C, the 70% ethanol will have enough concentration of ethanol vapors in the air to cause explosion in the presence of an ignition source. This ignition source can be provided by the electric discharge from various surfaces. Considering the present wide spread use of several low flash point organic solvents and large quantity of dry powders (a major source of tribocharging) in pharmaceutical, food, defense and nutraceutical industries, tribocharging raises major safety concerns.

Tribocharging has been known mostly to take place between different materials and has been found to increase with increased surface contact area, suggesting increased accumulation of specific charge for particles with smaller dimensions. Among the various surface factors affecting the polarity and magnitude of tribocharging includes roughness, contact force, friction, co-efficient of restitution, hygroscopicity, crystallinity and shape. However, bipolar charging has also been observed between particles of the same material with different size fractions. Bipolar charging in similar materials has predominantly been observed to trigger tribocharging [14–22] in a way where smaller particles tend to acquire negative charge on coming in contact with bigger counterparts, which acquire positive charge. Tribocharging in identical materials has been observed in various fields ranging from i) pharmaceutical unit operations such as fluidized bed drying [15], and pneumatic conveying [14]; ii) natural phenomenon such as dust storms [18–20,22] and volcanic plumes [21]; iii) aerosols such as found in DPIs [16]; and iv) Mars regoliths [17] etc. This phenomenon has also been confirmed through various experimental set-ups, and the magnitude of charge is found to increase with a concomitant increase in particle size ranges [23,24]. Some of the earliest experimental evidence of bipolar charging in identical materials can be traced back to 1957, when Henry [25,26] reported different polarities of charge on two similar rods, and the polarity of charge was based on their position as a bow or string of a violin.

Conductor or metal contact electrification has been studied for many years and is well understood to be a process of the transfer of electrons between two metal surfaces, driven by the difference in chemical potential of the interacting materials to achieve thermodynamic equilibrium [27]. But a consensual theory to describe insulator–metal or insulator–insulator contact driven tribocharging is still missing, considering the insulator surfaces are not well characterized. The three most widely accepted hypotheses for the same are as follows: i) *Electron transfer*: advocating the procurement of positive or negative charges based on the lower or higher ionization potential values respectively [28–31]; ii) *Ion transfer*: advocating the transfer of charge to and from insulators with the help of mobile ions [32–35]; and iii) *Mass transfer*: advocating the transfer of mass from a soft material (polymer) to a rougher and harder material (metal) [36,37]. The effects of electron transfer have often been regarded as the main charging mechanisms in case of non-ionic polymers in absence of the mobile ions [2,28,29]. However, what is more intriguing is how to define the charge transfer mechanisms in identical materials. Since its first observation, many literature reports and hypotheses have been published to describe this phenomenon. In 1985, Lowell and Truscott [38] made an attempt to explain this phenomenon using various experimental procedures ranging from sliding a ball over a plane in both vacuum and atmosphere, and they came up with a mathematical model based on the non-equilibrium distribution of energy states to describe the same [39]. Recently in 2008, Lacks et al. have embarked on the same principle and have mathematically demonstrated the viability of this non-equilibrium state model [40]. However, it is necessary to explain the energy distribution of electron states at the surface of insulators [39], otherwise limiting its physical understanding and hence failing to provide ways to mitigate bipolar charging in real scenarios.

The fact that the insulators are not ideal insulators and there are trapped electrons in the band gap [40] available to be transferred to lower energy states, allows scope of metal-like work function treatment of the insulators to predict charge transfer and develop a triboelectric series. Similar treatments could also reveal surface work function differentials between different size fractions of identical materials. Recently Murata [41] and Zhao et al. [42] have discussed the effects on work function values in different polymers based on the depth of the surface electronic states, the trap densities and the distribution of the filled states. Zhao et al. [42] have discussed the effects of surface roughness on tribocharging, i.e. different amounts of surface roughness can lead to different amounts of adsorbed species and hence different extent of contact and charge transfer. Li and Li [43] observed a decrease in work function in metals with increase in physical properties like plastic strain. Brocks and Rusu [44] investigated the changes in work function due to atmospheric contamination or chemisorbed surface species, by altering the surface dipoles based on the intrinsic dipoles of the molecules of the absorbed species. Cartwright et al. [14] have also discussed the effects of surface moisture on bipolar charging of polyethylene powder and determined that the relative humidity (RH) plays a significant role in determining the polarity as well as the magnitude of the charges generated.

All the afore-mentioned theories and discussions have been around for some time, but they still lack a satisfactory explanation for tribocharging in identical insulator materials. In the

course of this study an attempt has been made to predict the work functions of the different materials under consideration and correlate these properties to verify tribocharging in insulators through both experiments and simulations. Experiments of granular flow in a simple hopper chute assembly were performed on two different sizes of microcrystalline cellulose (MCC) non-pareils to study the charge variations against different chute wall materials, a metal (Al) and an insulator (PVC). Analytical tools were further implemented to study the variations in surface properties based on particle size differences of the excipients and hence an effort has been made to calculate the changes in work functions due to differences in surface properties using computational tools. The work functions obtained through quantum calculations were incorporated in the Discrete Element Method (DEM) algorithm pertinent to model bulk granular flow [45] to predict the charge profiles in hopper chute assembly and further validate the simulation data with the experimental results.

2. Materials and methods

2.1. *Experimental and analytical methods*

The hopper chute experiments were performed on both the homogeneous system and the binary mixtures of MCC. Two different sizes of MCC [MCC 700 (Sieve 25) and MCC 1000 (Sieve 16)] non-pareils were implemented for tribocharging experiments to reduce variability in size fraction and were further analyzed during the analytical experiments to determine differences in surface properties between different sizes of same materials. These excipients were systematically sieved to produce narrow and accurate particle size fractions.

2.1.1. *Flow and tribocharging experiments in hopper-chute assembly*

All hopper-chute flow experiments were performed in a RH controlled glove-box where the required humidity is maintained by re-circulation of air (Fig. 1). Air from the glove box is re-circulated using a dual air pump that draws air from one side and delivers it through the other side in the glove box. The air, which is delivered by the air pump, goes through a series of steps before entering the glove box. First air passes through a pressure gauge that records its current pressure, after which it is divided into two paths each controlled by a solenoid. These solenoids regulate the percentage of air passing through dry-canisters or nebulizer in order to maintain required humidity inside the glove box. All the hopper-chute experiments were performed at 20 ± 2.5% RH.

Hopper chute assemblies were designed in two different materials i.e. aluminum (Al, a conductor metal) and polyvinyl chloride (PVC, a polymer/insulator). All non-pareil particles were initially loaded into the hopper followed by de-ionization using the de-ionizers (Model 970, Meech Static Eliminators, Ohio, USA) mounted in the glove box. The de-ionized particles were then released through a 1 cm slit by disengaging the dam of the hopper and allowing them to flow on a chute at an angle of 30° with respect to the horizontal axis of the hopper. At the end of the chute, the particles were collected in a faraday cup (284/22B 6" Diameter Faraday Cup from Monroe Electronics, New

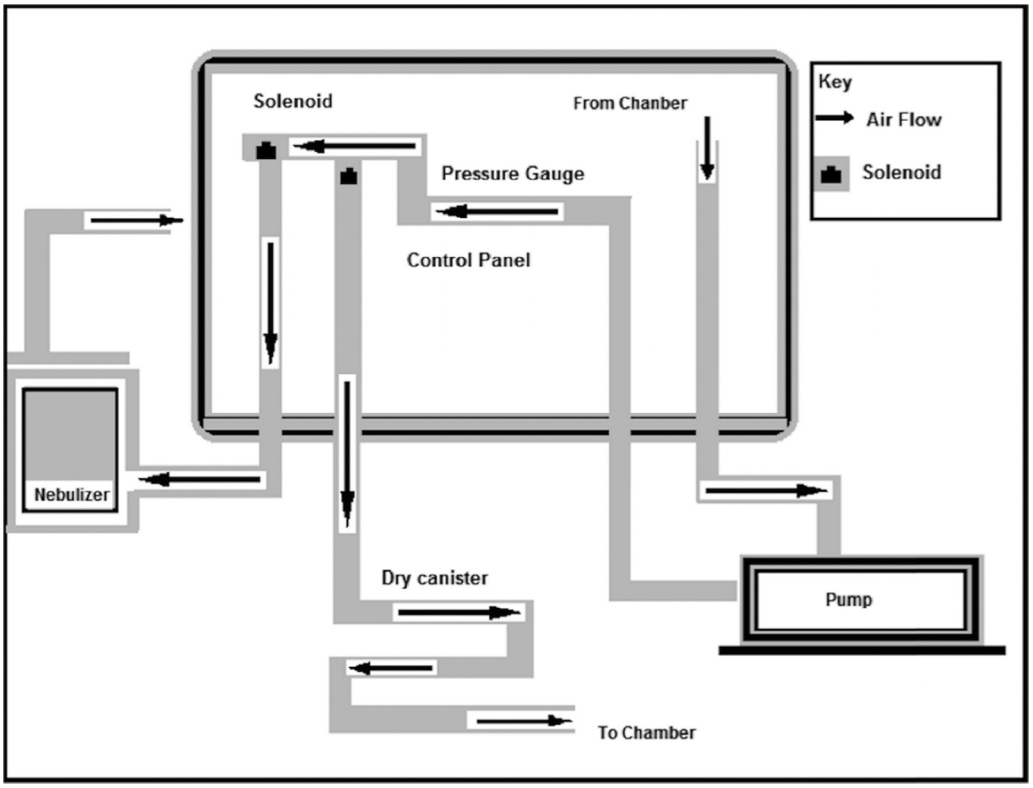

Fig. 1 – Schematic illustration of the Humidity controlled glove box.

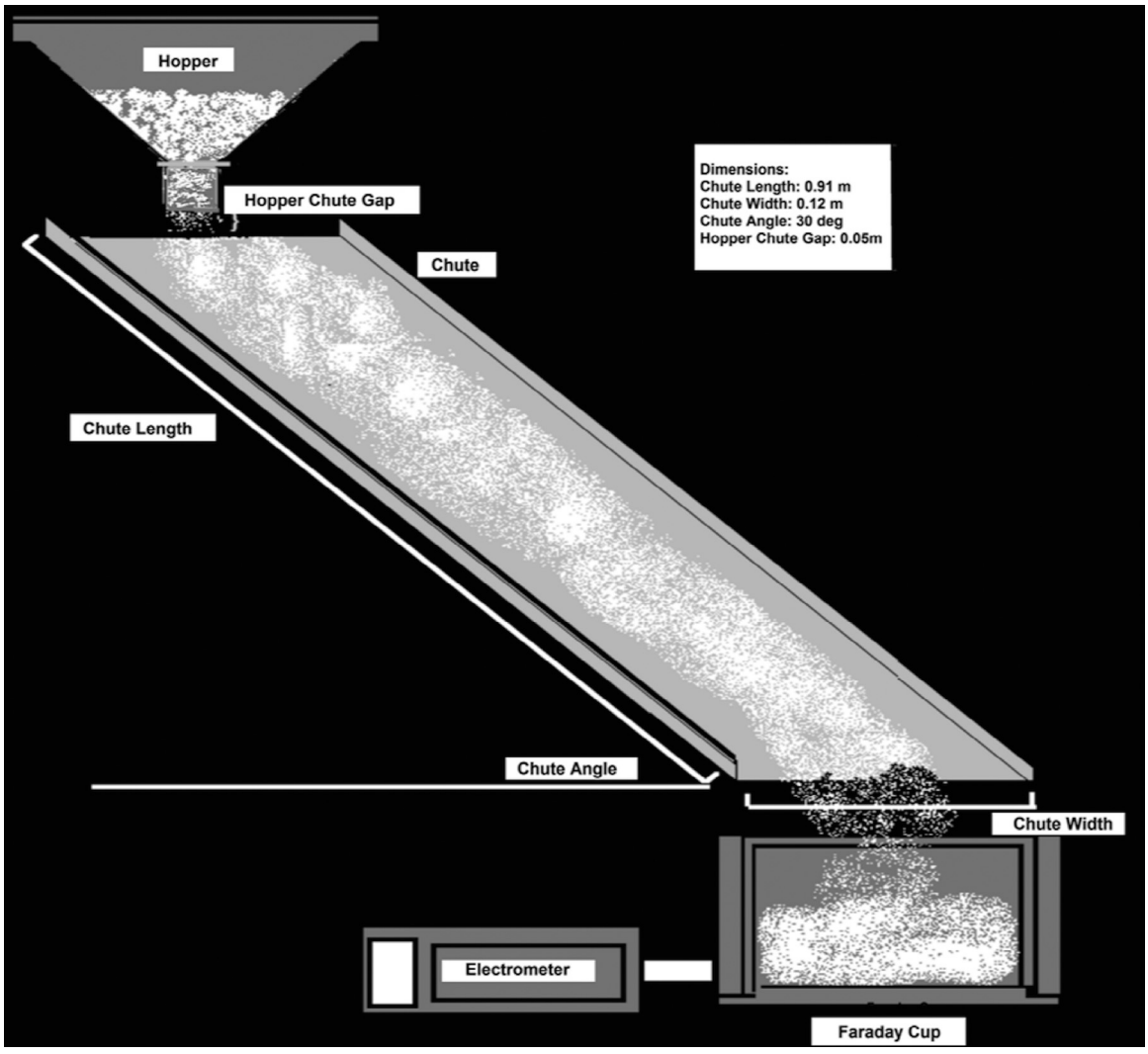

Fig. 2 – Experimental set-up: Hopper-chute assembly.

York, USA) as shown in Fig. 2, and the charge was recorded with the help of a Nano-Coulomb Meter (Model 284, Monroe Electronics, New York, USA). The masses of the non-pareils collected in the faraday cup were measured after each run to estimate the charge/mass values. Experiments were performed multiple times to reduce any relative standard deviation.

2.1.2. *Analytical techniques*

Multiple analytical techniques were performed to analyze differences between different particle size fractions of the same material. Profilometric studies were performed using Zygo-3D optical interferometer profilometer. All the sample surfaces were initially sputter coated with ca. 100 Å thick gold layer to increase the reflectance of polymeric surfaces in order to obtain better signal to noise (S/N) ratio. Microscopic imaging of above mentioned samples was performed using JEOL JSM-6335F scanning electron microscope (SEM). All the sample surfaces were initially sputter coated with ca.100 Å thick gold layer to increase the conductance of their respective surfaces, and hence enabling the SEM imaging of the same. Surface elemental composition was studied on all the surfaces using x-ray photoelectron spectroscopy unit of PHI 595 multi-probe system. Aluminum and magnesium twin x-ray source was used to produce x-ray beam of 1486.6 eV. Survey spectra were collected for all the surfaces for binding energies ranging from 0 eV to 1100 eV. RBD Instrument interface and software was used to qualitatively and quantitatively analyze all the peaks. The atomic percentage for each element on the surface was calculated based on its peak area and its sensitivity factor for XPS. Bulk elemental composition was studied using Thermo Noran System Six EDS (Thermo Scientific, USA).

Thermogravimetric analysis was performed on both MCC non-pareils using TGA Q-500 (TA Instruments, New Castle, DE). The thermal stability of the material was studied by increasing the temperature from 25 °C to 600 °C at a ramp rate of 20 °C/min. Dynamic vapor sorption studies were performed on DVS 2/2000 by Surface Measurement Systems, which is an automated dynamic vapor sorption (DVS) analyzer to predict the moisture contents at different RH conditions. The mass flow controllers were used on dry nitrogen line and saturated water vapor line to achieve the desired humidity from 0% to 70%. The temperature was kept constant at 25 °C during the runs and the DVS 2.17 software was used to monitor the signal change during the humidity step change. About 10 mg of

each test sample was loaded into the sample pan followed by equilibration at increasing RH, and the change in weight at different RH was measured using the ultra-sensitive microbalance.

2.2. *Multi-scale computational methods*

2.2.1. *Work function analysis*

The work function is the minimum energy or the thermodynamic work needed to extract an electron from a solid material surface. The concept of work function differential has often been investigated for insulators either through experiments or using *ab initio* DFT (density functional theory) or from semi-empirical molecular orbital calculations. In our present study the work function (φ) [46] of the molecule has been determined in terms of ionization potential (IP) and energy gap (E_{gap}) between HOMO (Highest Occupied Molecular Orbital) and LUMO (Lowest Unoccupied Molecular Orbital) and has been expressed as [2,46]:

$$\varphi = IP - \frac{1}{2}(E_{gap}) \tag{1}$$

In the course of our study, it was necessary to understand whether the adsorbance of moisture on the excipient surfaces could lead to changes in work functions of materials and hence in charging tendencies. Density Functional Theory (DFT) was used to estimate the drop in work functions of the materials due to adsorption of water on the material surface. The first-principles based computation was performed within the framework of dispersion-corrected density functional theory (DFT-D2), using the projector augmented wave method as implemented in the Vienna *ab initio* simulation package [47–49]. In the present calculations, the exchange correlation interaction was treated within the generalized gradient approximation (GGA) using the Perdew–Burke–Ernzerhof (PBE) functional [50–52]. The electronic wave functions were expanded in a plane wave basis with a cut off energy of 400 eV. The slab was separated by a vacuum spacing of 12 Å, chosen by testing the variation in total energy with vacuum distance and the decay of the local potential away from the surfaces. During geometry relaxation a Γ-centered $5 \times 3 \times 1$ k-point mesh was considered. The gas phase energy of water molecule was calculated using a $10 \times 10 \times 10$ Å unit cell with a $1 \times 1 \times 1$ k-point sampling. It is worth mentioning that the cellulose chains are composed of ordered regions (nano-crystalline) and disordered regions (amorphous). Known polymorphic forms of cellulose are Iα and Iβ. Being thermodynamically more stable phase, Iβ has been studied in present work to get a qualitative understanding of cellulose–water interaction. To construct the slab atomic coordinates, structural details are taken from literature [53]. Semi-empirical methods, to predict the HOMO and LUMO energies of the moisture free material, have been adopted to calculate the work functions. Semi-empirical calculations [2,54] were performed using MOPAC 2013 from structures generated with AVOGADRO 1.0.3 [2] with Restricted Hartree–Fock (RHF) PM3 methodology to calculate the work functions of the materials used in our experimental approach.

2.2.2. *Discrete Element Method (DEM)*

The Discrete Element Method (DEM) was first implemented by Cundall et al. [55,56], and since then has been extensively used to understand particle dynamics in multiple pharmaceutical manufacturing processes including hopper discharge [57], milling [58], flow in rotating drums [59], chute flow [60–62] etc. Initially, spherical, inelastic, frictional particles were deposited in the non-discharging hopper of same dimension to that of the experiment. DEM Simulations of homogeneous particles on both PVC and Al chute were performed. The particles studied through DEM simulations were designated with properties similar to that of MCC non-pareils, and the particle size radii were maintained at 750 μm (R750) and 1000 μm (R1000) to replicate the particle dynamics as observed in experiments. The increased sizes of the particles were implemented to reduce the computational demand, and since charge was normalized in terms of mass, the final specific charge (charge/mass) values were not compromised qualitatively. The particles were allowed to flow through the chute and were collected in a faraday cup at the end of the chute similar to the experiments. The charge to mass ratio could be calculated for all the particles collected in a faraday cup, since simulations provided us with the number of particles in the faraday cup and their individual charge and weight. Once particles have touched the surface of the faraday cup, they were made static to prevent any bouncing of the same.

2.2.2.1. *Modeling of particle dynamics*. The Discrete Element Method tracks the evolution of trajectory of individual particles by calculating all the forces acting on it, followed by integration of Newton's second law of motion, to obtain the new position and orientation of the particle. The DEM accounts for the position and orientation change of the particles at every small time step, and initializes the new co-ordinate set as the basis set for the calculation of the next time step. The net force (ΣF_i) on each particle is given by the sum of the gravitational force ($m_i g$) and the inter-particle forces (normal (F_N) and tangential (F_T)) acting on it, where m_i is the mass of the individual particle and g is the gravitational constant.

$$\sum F_i = m_i g + F_N + F_T \tag{2}$$

The corresponding torque (ΣT_i) on each particle is the sum of the moment of the tangential forces (F_T).

$$\sum T_i = r_i \times F_T \tag{3}$$

The normal forces (F_N) for inter-particle or particle–wall collision were calculated with the "partially latching spring force model" proposed by Walton and Braun [63]. The tangential forces (F_T) were calculated by the "incrementally slipping friction model" proposed by Walton [62] based on the force model proposed by Mindlin and Deresiewicz [64].

2.2.2.2. *Modeling of the electrostatic flow behavior*. The charge transfer mediated by continuous particle–particle and particle–wall collision was modeled in order to understand the electrostatic behavior of the particles and its impact on particle dynamics due to the changes in the net forces acting on the particle. The charge transfer [2,65] between the particle i and the particle j during a single collision is given by Δq,

$$\Delta q = \frac{\varepsilon_o S}{z q_e}[\varphi_i - \varphi_j] \quad (4)$$

where ε_o is the permittivity of free space (8.854×10^{-12} F m^{-1}), s represents the contact area, z is the cutoff distance for charge transfer considered to be 250 nm [66], and q_e is the charge of an electron (1.602×10^{-19} C). The charge transfer takes place only when $\varphi_i \neq \varphi_j$ and at the time step with maximum impact forces [67,68] between the particles. The final charge (q_{final}) has been calculated as,

$$q_{final} = q_{initial} \pm |\Delta q| \quad (5)$$

depending on whether $\varphi_i > \varphi_j$ or $\varphi_i < \varphi_j$. The charge transfer between the wall and the impacting particle has been modeled similarly, and the net charge on any particle at each time step has been assumed to be distributed homogenously. The introduction of electrostatic charge into the DEM algorithm requires addition of electrostatic forces that work in conjunction with the existing contact mechanics model. The Columbic force [65] (F_c) acting on a particle with charge q_i due to the presence of another particle with charge q_j is given by,

$$F_c = \frac{q_i q_j}{4\pi\varepsilon_o r^2} \quad (6)$$

where r is the distance between the particles. In order to predict the exact transformation in particle dynamics due to the non-homogenous charge density and spatial resistance across the system, an effective Screened Columbic [69,70] (F_{sc}) force has also been computed based on the approach by Hogue et al. in 2008. A Screened Coulomb force (F_{sc}) will be experienced by each particle with charge q_i separated by distance r from another particle q_j for the presence of other charged particles in closer vicinity.

$$F_{sc,i} = \frac{q_i q_j}{4\pi\varepsilon_o}\left(\frac{\tau}{r} + \frac{1}{r^2}\right)e^{-\tau r} \quad (7)$$

where τ is expressed as,

$$\tau = q_e\sqrt{\left(\frac{1}{K_B T \varepsilon \varepsilon_0}\sum_i n_i z_i^2\right)} \quad (8)$$

where ε is the relative permittivity of the medium, T is the temperature in Kelvin, K_B is the Boltzmann's constant (1.38×10^{-23} JK^{-1}), and n_i is the number of particles with charge z_i within the screening distance [2,69]. The net force acting on each particle is,

$$\sum F_i = m_i g + F_N + F_T + F_{sc,i} \quad (9)$$

3. Results and discussion

3.1. Hopper-chute flow

In our study to investigate the triboelectric variations due to particle size differences, the effects of second material interactions were inspected on both homogenous systems and mixtures. The hopper-chute flow system was chosen since it ascertains maximum particle–chute (second body) interaction as compared to particle–particle interactions. By maximizing the secondary material interaction and minimizing the particle–particle interaction in the hopper-chute setup, we can study the effects of the chute interactions on individual particle size fraction and correlate these studies to understand the effects of bipolar charging in identical materials in presence of multiple size fractions. Fig. 3 represents the specific charge profile of different concentrations of MCC 700 and MCC 1000 interacting with either Al or PVC chute wall. The SPF represents the small particle fraction (i.e. fractional concentration of MCC 700 in the mixture), where SPF = 0.0 represents a homogenous system of MCC 1000, and SPF = 1.0 represents a homogenous system of MCC 700. The higher specific charge in MCC 700 compared to MCC 1000 against both the chute walls could be attributed to the greater specific surface area allowing more contact with the chute wall material. The charge acquired through particle chute interactions dominated the flow regime, and the polarity of the charge obtained was positive or negative based on the chute wall material, i.e., PVC and Al respectively. The fact that most incidences of bipolar charging have been studied or reported in fluidized systems [14,15,71] (such as fluidized beds, tornadoes, pneumatic conveying, etc.), where particle–particle collisions largely exceeds particle–wall interactions, points to the fact that any bipolarity obtained due to particle–particle interactions could be suppressed by dominant charge transfer due to the particle–wall interactions. However, the non-linearity in the acquired charges with the gradual increase of SPF indicates interactive charge transfer parameters beyond particle–chute collisions. A drop in the net specific charge was obtained for the 1:1 mixtures (SPF = 0.5), which allowed maximum particle–particle interactions. Fig. 4 represents the mean percentage charge variations at different SPF conditions relative to SPF = 1.0, indicating a maximum charge drop at SPF = 0.5. However, it is complicated to separately obtain the different particle size fractions in the hopper chute assembly, without secondary material

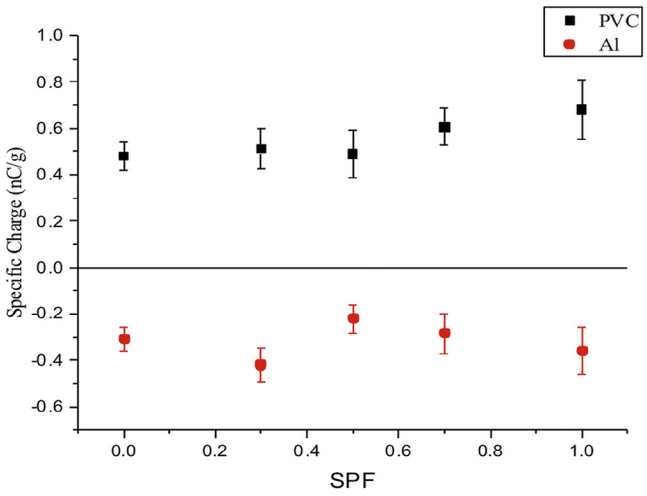

Fig. 3 – Specific Charge profile of MCC 750 and MCC 1000 against PVC and Al chute wall.

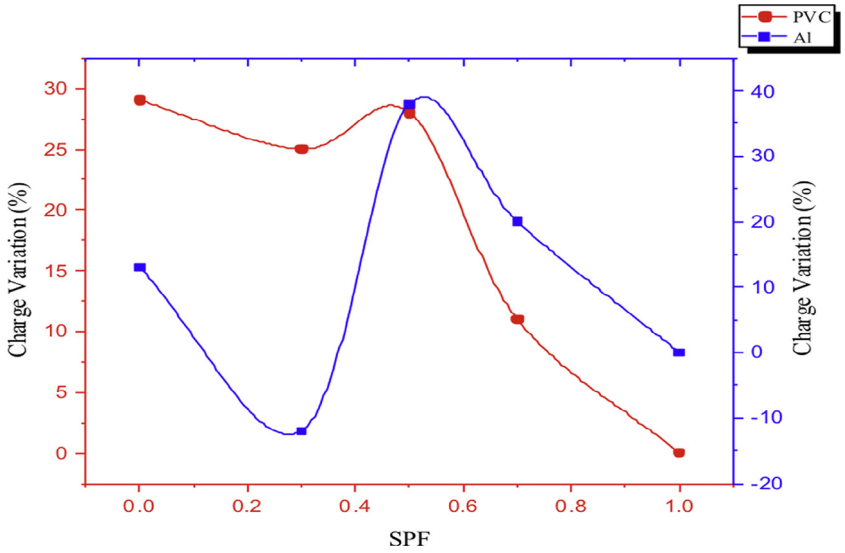

Fig. 4 – Mean Specific Charge variation at different SPF conditions against PVC and Al chute walls.

interferences. Hence, in order to correlate our experimental observations to predict the phenomenon of bipolar charging in identical materials, it was necessary to computationally model the experiments and validate the bipolarity by identifying the charge on individual size fractions and the specific charge of the system at the final time step.

Table 1 – The root mean square roughness values for different sizes of MCC 700 and MCC 1000.

Non-Pareils	Roughness (μm)
MCC 700	2.00
MCC 1000	1.72

3.2. *Analytical techniques*

Surface topography of both MCC particle sizes was studied with the help of two complimentary techniques i.e. Optical Scanning Interferometer-Profilometry and Scanning electron microscopy (SEM). The Interferometer-Profilometer was used to analyze the surface roughness (Fig. 5A and 5B), followed by SEM analysis to compliment the same and additionally to observe the surface defects and other topographic features. Profilometric studies as shown in Table 1 suggested slightly higher surface roughness for smaller particles (MCC 700). The SEM images as shown in Fig. 6A and Fig. 6B were found to be in agreement with the observations made with profilometric studies. The greater surface roughness of MCC 700 was in accordance with the observations of Zhao et al. [42]. Their hypotheses on acquiring bipolar charges in identical materials were based on the work function changes due to preferential adsorption of atmospheric impurities based on differences in surface roughness values. Both the surface and bulk impurities were analyzed using XPS and EDS techniques respectively. Surface impurities can trigger triboelectrification by altering the effective work function of the materials, by changing the mode of interactions between different particles, or by taking part in transfer from one surface to another [25,26,38]. The bulk impurities were analyzed since they can affect the process of tribocharging if they are within charge penetration depth (CPD) region as described by Williams [72]. The XPS analysis on two

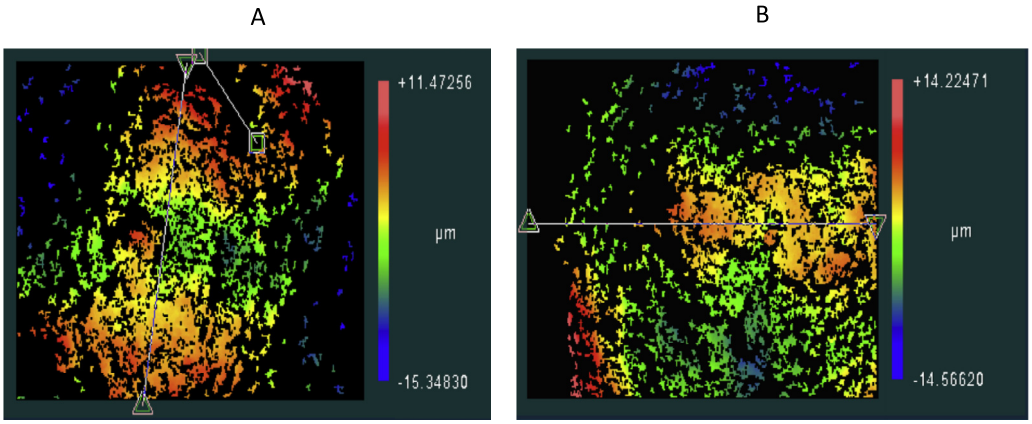

Fig. 5 – Surface Roughness studied by Interferometer Profilometer on (A) MCC 700 and (B) MCC 1000.

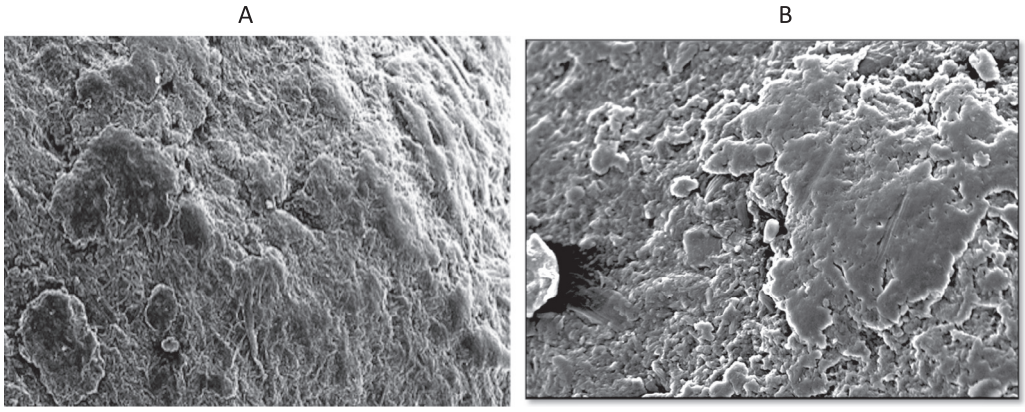

Fig. 6 – Surface Topography studied by Scanning Electron Microscope on (A) MCC 700 and (B) MCC 1000.

different sizes of MCC particles revealed MCC 700 adsorbing 1% of total atomic percentage as silicon, whereas MCC 1000 demonstrated absence of any impurities on their surfaces. This indicates randomness in the amount and type of impurities present on material surfaces. The consistency and content uniformity of the adsorbed species are highly variable and will be majorly dependent on the exposed atmosphere. Since the phenomenon of bipolar charging (where smaller particles are consistently observed to be negatively charged) in identical materials has been consistently observed in different experiments and manufacturing processes irrespective of atmospheric exposure, it would be hard to explain it as a site and time specific random process based on surface impurities from atmospheric contamination. EDS analysis performed on different samples revealed the absence of any bulk impurities for both smaller and bigger sized particles. Absence of impurities in the bulk and in the CPD region facilitates us to neglect any effects on work functions from differences in the bulk composition of different sized MCC particles.

Moisture content of the specified material was estimated using both Thermo Gravimetric Analysis (TGA) and Dynamic Vapor Sorption (DVS) techniques. Initially TGA was performed to estimate their degradation temperature and analyze the total volatile content of the same. The degradation temperature observed for MCC was ca. 280 °C and was found to be stable until at least a temperature of 200 °C; it was chosen as the isothermal temperature for estimating the total volatile content of these materials. The total volatile content for MCC particles was found out to be 5% of its total weight. To further confirm the above findings and to extensively study the amount of moisture sorption for different particle sizes of each material, a thorough Dynamic Vapor Sorption (DVS) analysis was performed as explained earlier. The results obtained were interpreted in terms of amount of moisture content per unit area (millimoles/cm^2), considering the focus of our study to be charge transfer between individual particles. Non-pareil diameters for all the particles implemented for DVS studies were individually measured. DVS analysis revealed increased surface moisture sorption and hence increased number of moles of moisture per unit area for MCC 1000 as compared to MCC 700 at different RH conditions (Table 2). This can be attributed to increased scope of surface moisture sorption capacities of individual MCC 1000 to MCC 700 particles. This difference in the moisture content on the particle surfaces of the same material but different sizes could be the key to solve the ambiguities of bipolar charging, since trends in moisture content will be more consistent at specified RH in comparison to other impurities. Hence, if differences in water sorption can be related to mechanisms regulating charge transfer, maybe we can explain and quantify the unexplained avenues of bipolar charging and come up with ways to mitigate this problems by implementing necessary precautions.

3.3. *Work function calculations*

Quantum calculations based on Density Functional Theory (DFT) were performed to study the effects of surface water adsorption on the work function of MCC. To study the differences in work functions of the material, calculations were performed to predict the effective differences in ionization potential (IP) and the (LUMO-HOMO) energy gap (E_{gap}), with and without the introduction of the water molecules. The effective difference for slabs with adsorbed water revealed lower energy differences between (IP) and (E_{gap}), hence projecting a drop in the work function of the system by 0.21 eV. In order to elucidate the interaction mechanism between the cellulose chains and water molecules in the crystalline regions, we considered only a small number of molecules. We found an immediate formation of a hydrogen-bonding network occurring between cellulose and OH^- dispersed in the interstitial regions. The present DFT based study suggests that on the surface, the dissociative adsorption of water molecule is favored as the unsaturated surface terminal CH_2 (via strong H-bond) attracts one of the hydrogen from water molecule and water molecule breaks into a H^+

Table 2 – The Dynamic vapor sorption analysis results in terms of millimoles of water per unit surface area (cm^2).

RH (%)	Moisture [MCC 700] (millimoles/cm^2)	Moisture [MCC 1000] (millimoles/cm^2)
10	0.9	1.1
20	3.3	3.5
45	26.9	32.5
70	55.3	70.7

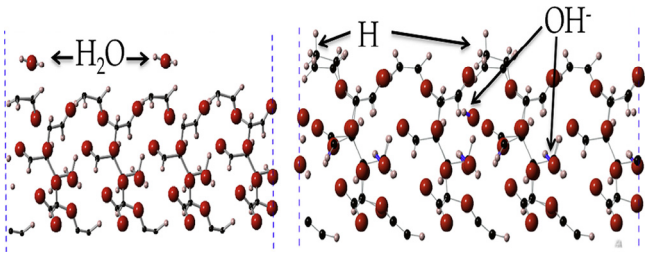

Fig. 7 – MCC slab before and after moisture sorption.

and an OH^- group (Fig. 7). During the water dissociation process, H atom attached to the surface terminal oxygen forms a short (less than 1.5 Å) hydrogen bond with oxygen of OH^- group. The polar bonding may occur inter-molecularly (between different cellulose) as well as intra-molecularly (within different parts of single cellulose). The hydrogen bond is often described as an electrostatic dipole–dipole interaction. Moreover, it is directional and strong, and results into shorter interatomic distances than sum of the van der Waals radii explaining the lower value of DFT calculated work function. The work function values were calculated in the order PVC > MCC > MCC (with adsorbed moisture) > Al (Fig. 8). As per the work function calculations, greater water sorption on particle surfaces should lead to lowering of their work-function values. The lowering in work-function values facilitates the attainment of greater positive charge on the particle surfaces (MCC), indicating a potential basis of bipolar charging in identical materials.

3.4. *Simulation results*

The DEM algorithm tracks the kinematics and charge of each individual particle, revealing myriad of information barely available in experimental analysis. The electrostatics algorithm [2] explained in Section 3.2 was incorporated in a previously developed 3D-DEM code [45] in order to validate the tribocharging observations in our experimental setup. The system properties for each of MCC particle size fractions were incorporated in the algorithm (Table 3) to verify the magnitude and polarity of the charges obtained in our experimental analysis, depending on the chute wall material (Al and PVC). The simulations were performed for radii 750 μm (R750) and 1000 μm

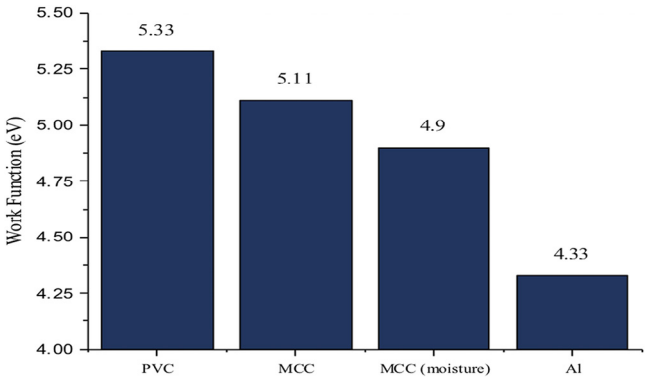

Fig. 8 – Work function analysis of the excipients and chute materials.

Table 3 – The DEM parameters employed for particle dynamics simulations.

Parameters	R1000	R750
Radius (μm)	1000	750
Number of particles (Homogenous system)	1600	3800
Work Function (eV)	4.90	5.11
Coefficient of restitution (particle/wall)	0.5	0.5
Coefficient of restitution (particle/particle)	0.6	0.6
Frictional coefficient (particle/wall)	0.5	0.7
Frictional coefficient (particle/particle)	0.6	0.6
Stiffness Coefficient (N/m)	1000	1000
Hopper Angle (°)	45	45
Chute Angle (°)	30	30
Time Step (seconds)	5.00E-07	5.00E-07

(R1000) with varying SPF (0.0, 0.3, 0.5, 0.7 and 1.0), where SPF in the simulation represents the fractional concentration of R750. The work functions were introduced in our electrostatics model for the materials, as obtained from the work function calculations. As mentioned earlier, the large particles were assigned a lower work function based on the assumption that they have higher number of moles of surface moisture. The DEM model was capable of predicting both inter-particle and particle–wall charge transfers, and it was essential to understand if the final specific charge could be correlated to the dominant particle–wall interactions.

The DEM results were in accordance with our experimental observations, as the final specific charge in each of the hopper-chute system was dependent directly on the chute wall material as shown in Fig. 9. The homogenous systems showed similar patterns as to the experiments, with higher net specific charge for particles with smaller dimensions. The polarity of the charges obtained for the hopper chute simulations was positive or negative based on whether the chute wall was PVC or Al respectively. To confirm if the charge transfer mediated by the dominant chute wall interactions suppressed the polarity induced by the bipolar charging, mixtures of R750 and

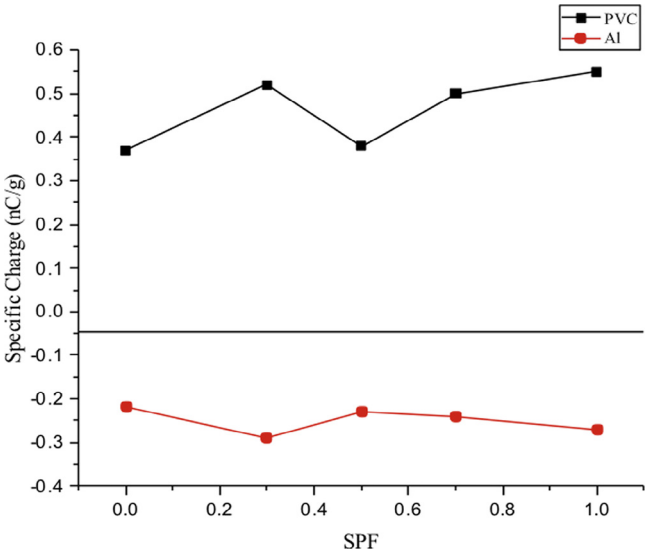

Fig. 9 – Simulation results of the specific charge profile of R750 and R1000.

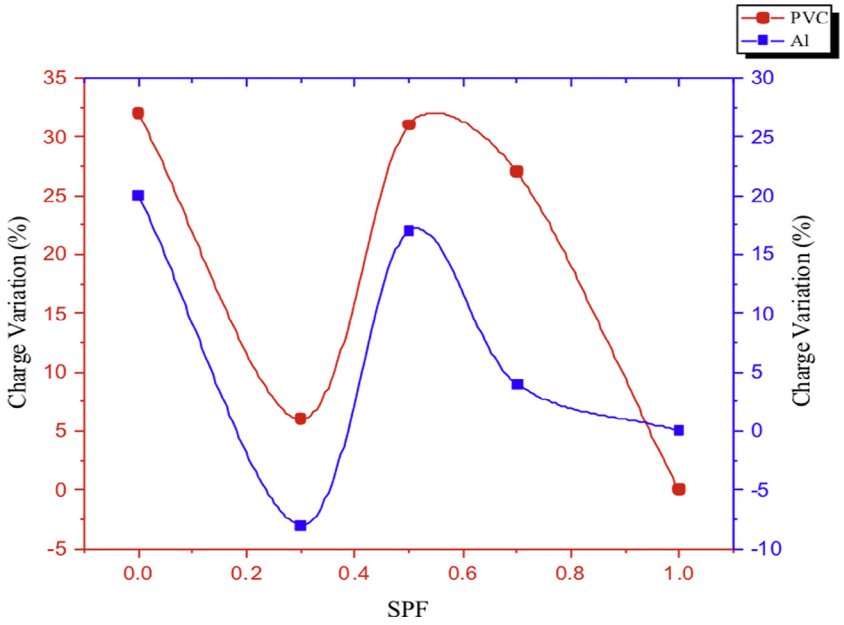

Fig. 10 – Simulation results of mean Specific Charge variation at different SPF conditions against PVC and Al chute walls.

R1000 (SPF 0.3, 0.5 and 0.7) similar to experiments were studied. The charge transfer between R750 and R1000 particles was mediated by moisture induced work function differences. The polarity of the final specific charge of the system was in accordance with the net specific charge obtained from the experimental results, and predicted the non-linearity of acquired charge with increase of SPF (Fig. 10). However, the DEM algorithm allows to calculate the charge profile on each individual particle and thereby confirmed the particle–particle interaction mediated bipolarity. In the simulation mixtures, as per predicted by the work function differences we observed bipolar charging, with the large particles (R1000) getting positively charged and the small particles (R750) getting negatively charged, irrespective of the chute wall materials. Fig. 11 and Fig. 12 represent the charge profile of individual particle size fractions and the net charge of different mixtures (SPF = 0.3, 0.5, 0.7) against PVC and Al chute wall respectively. Based on the dominant particle wall interactions, the magnitudes of the specific charges were found to be the function of the work function differential between the particles and the wall material. The inequality of specific charges normalized with respect to surface area justifies the non-linearity of charge accumulation with the increment of SPF, suggesting probable explanations that remained unanswered from the experimental observations. Fig. 13 represents the variability of charge per unit area (nC/dm^2) for the homogenous system (SPF = 0.0 and 1.0) and

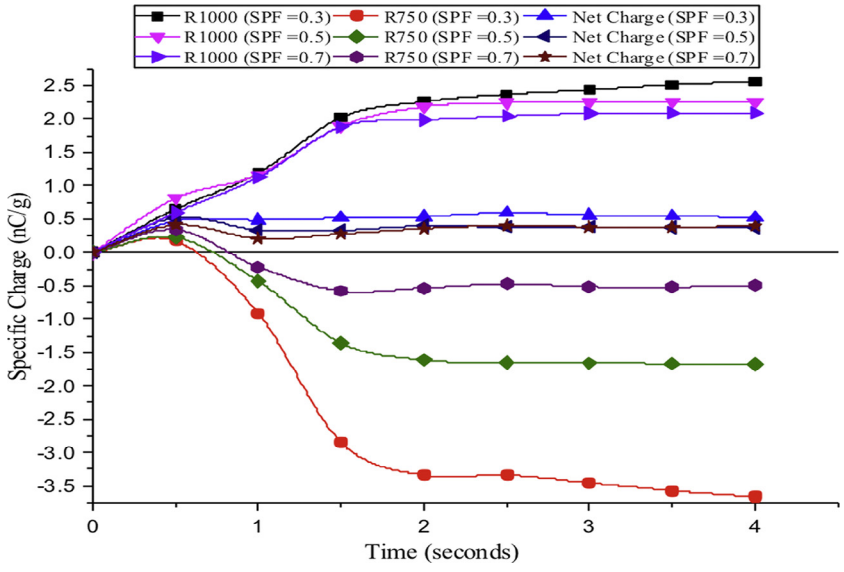

Fig. 11 – Simulation results of the specific charge profile of SPF = 0.3, 0.5 and 0.7 against PVC chute wall.

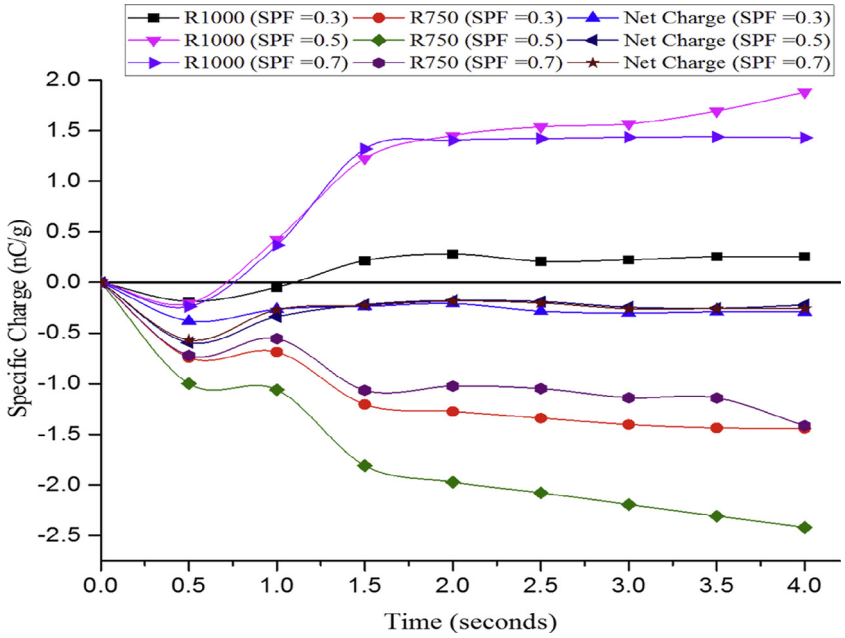

Fig. 12 – Simulation results of the specific charge profile of SPF = 0.3, 0.5 and 0.7 against Al chute wall.

1:1 mixtures (SPF = 0.5) confirming charge transfer as a phenomenon beyond simple functional of surface area. The particles have been color-coded based on the specific charge of each particle at particular time steps. Fig. 14(A–C) represents the MCC binary mixture at different concentrations against PVC chute wall, each suggesting the larger particles charging positively and small particles negatively. The maximum variation in polarity is prominent at SPF = 0.5, which allows maximum particle–particle interactions. The bipolar charging is present in SPF = 0.3 and 0.7, but less prominent compared to SPF = 0.5, due to increased domination of the particle wall impacts. Similar results were obtained against Al chute wall (Fig. 15 (A–C)). However, there were some differences in the magnitude of the charges between the experiments and the DEM models (Fig. 16), probably because the DEM simulations were modeled to predict the charge transfer between particles of the same materials, but considered only one of them to adsorb moisture, and the other size fraction to have null moisture absorbance, in order to study the effect of tribocharging due to differences in moisture content.

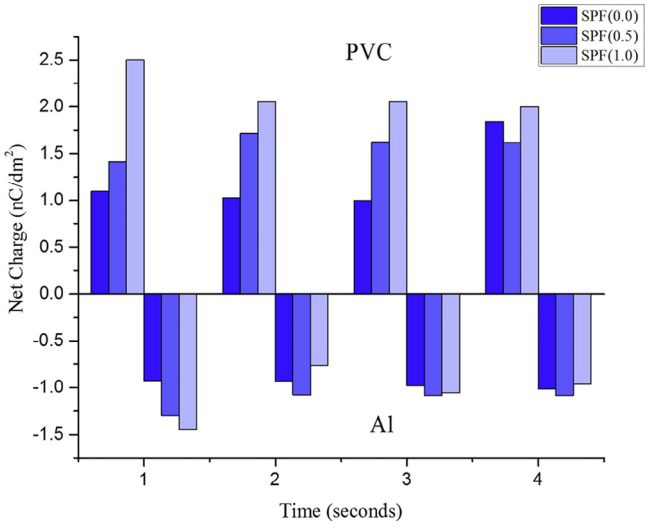

Fig. 13 – Simulation results of tribocharging as a function of surface area.

4. Conclusions

A thorough characterization and analysis of two different sizes of MCC non-pareils have been provided to study and understand the magnitude and polarity of acquired charges against both metals and insulator surfaces and also variation in surface properties that might unveil the causes of bipolar charging of identical granular materials during the processing. The differences in surface roughness obtained for the two size fractions were prominent in terms of net acquired charges on the surface of homogenous systems, with smaller particles acquiring higher magnitude of charge. However, the randomness in the amount of impurities present on smaller and bigger sized particles confirmed the lack of consistency to predict bipolar charging based on surface impurity content. The DVS studies were analyzed to predict the specific moisture content on individual particles, suggesting greater moisture content for MCC 1000 at different RH conditions. This provided a consistent basis of further prediction of variations in charge transfer capabilities leading to bipolar charging in identical materials. Computational tools were further implemented for i) Work–function calculations: which suggest lowering of work function with the adsorption of water molecules. ii) DEM simulations: confirmed increase of specific charge with decrease of particle sizes in homogenous mixture; however in binary mixtures, difference in moisture contents led to bipolar charging in identical materials, and the net specific charge for both homogenous

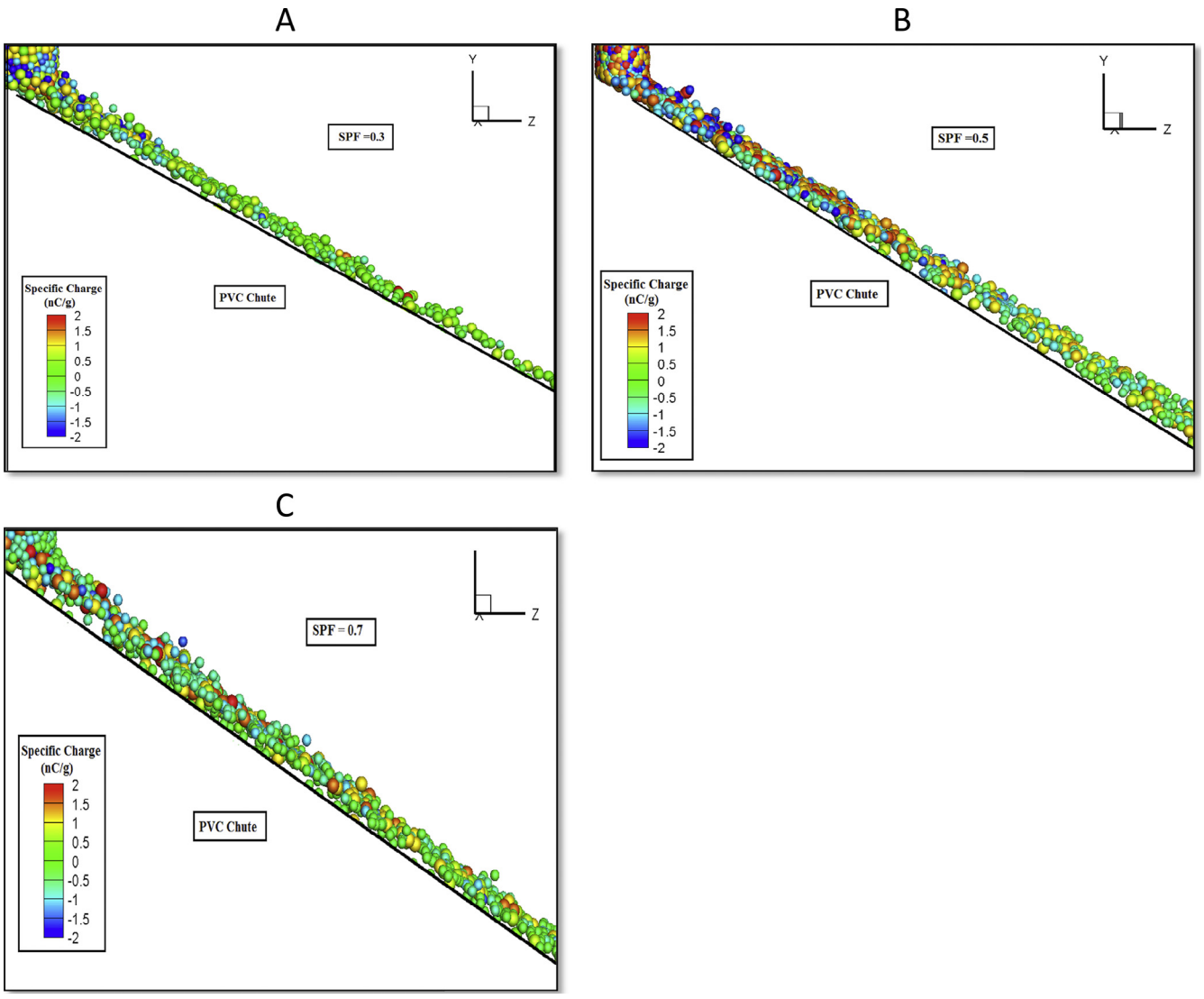

Fig. 14 – Simulation results of tribocharging of MCC mixtures against PVC: (A) **SPF = 0.3,** (B) **SPF = 0.5 and** (C) **SPF = 0.7.**

and binary mixtures was in conformation with the experimental results.

The final specific charge in the DEM model was found to be dependent on the chute wall properties and could barely reflect any bipolar interaction between the surfaces of the same material similar to that of the experiments, other than predicting the inconsistent behavior of charge increment with increase of SPF. However based on the difference in moisture adsorption and other analytical observations, a difference in surface property between particles of the same material could be clearly suggested. Based on the hypothesis that the alteration of surface property due to differences in surface moisture contents will alter the work function of the material, the DEM simulations clearly suggested bipolar charging in particulates in the hopper chute experiments. Discrete studying of individual particles allowed us to confirm bipolar charging in the hopper chute assembly, with large particles charging positively and small particles charging negatively. There are multiple interactions during a process, and each has its own implications regarding charge transfer, and the net effect might well not reflect the bipolarity phenomenon. As has been confirmed in fluidized systems, the interaction between similar particles leading to bipolar charging, the same phenomenon is also true for non-fluidized bed systems, and might lead to multiple manufacturing impediments like agglomerations, material loss or explosion hazards.

The explanations to bipolar charging are multi faceted, and any one hypothesis might not entirely explain the exactness of the phenomenon. The hypothesis that work function differences due to moisture adsorption lead to bipolar charging at lower RH provides a new avenue to explain the bipolarity in the same material and to predict the bipolar behavior in more complex systems with a wide range of particle size distributions. However, the experiments only measure the final or the net charges of the system and we cannot measure charges on individual particles. DEM overcomes the experimental limitations by performing multi-scale modeling to not only predict the total charge (as has been obtained from experimental analysis) but also individual particle based bipolarity.

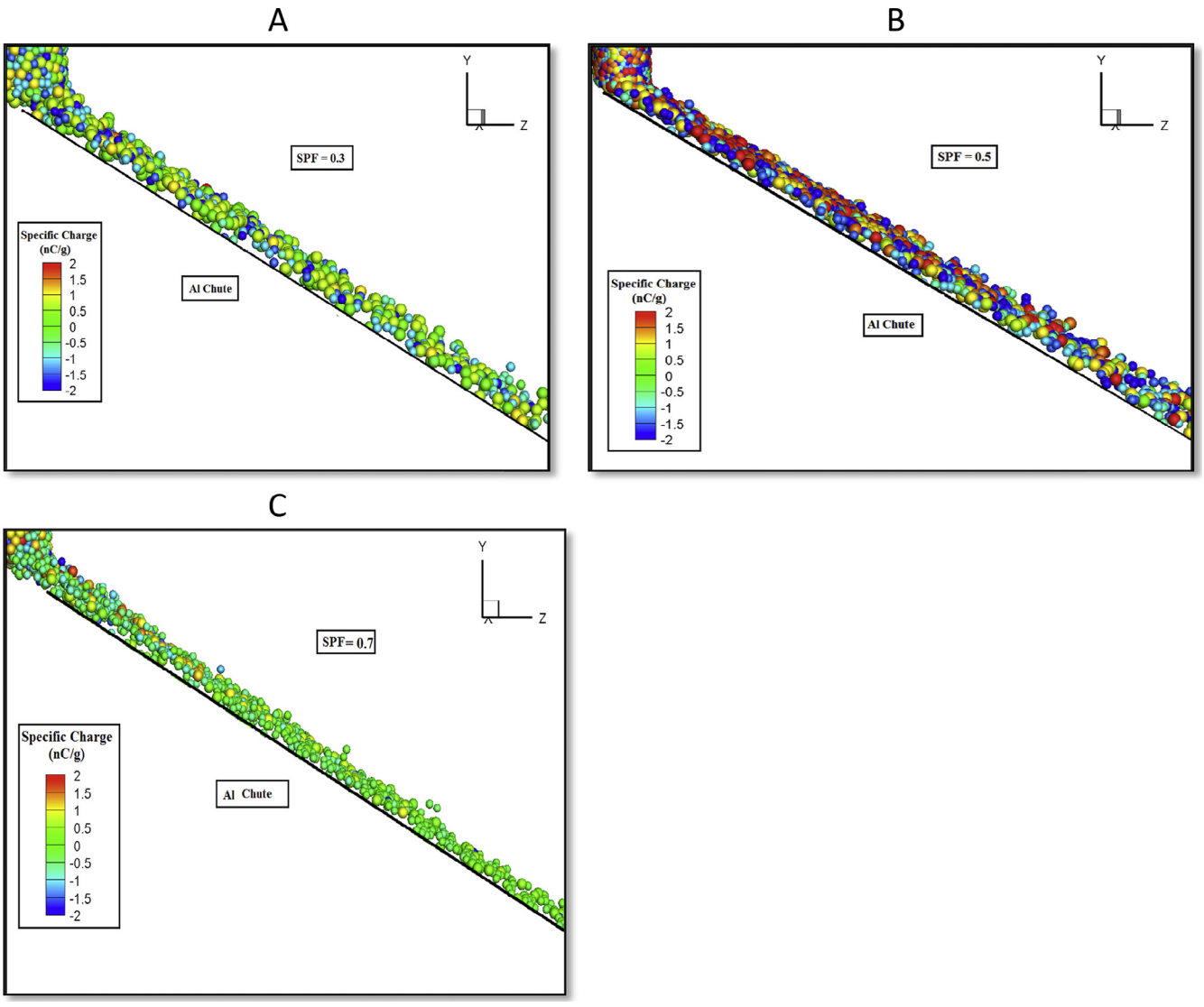

Fig. 15 – Simulation results of tribocharging of MCC mixtures against Al: (A) **SPF = 0.3,** (B) **SPF = 0.5 and** (C) **SPF = 0.7.**

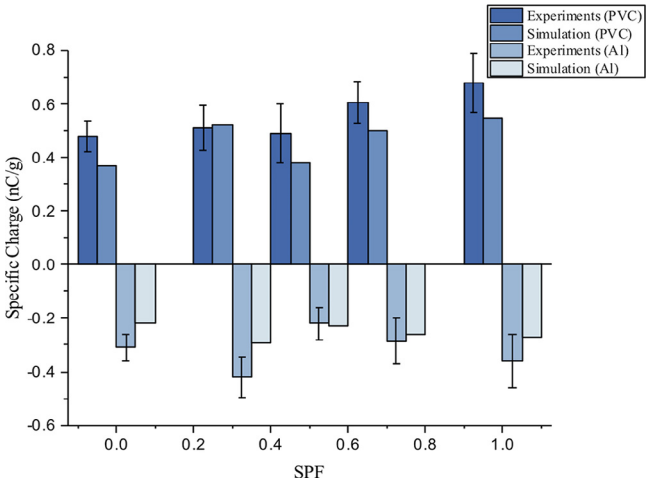

Fig. 16 – Comparative results of Experimental and Simulation data.

Acknowledgements

We would like to thank the U.S. Food and Drug Administration (Grant no. 5U01FD004275) for their support and funding. We would also like to thank the technicians of the Department of Mechanical Technology at University of Connecticut for assisting us with the experimental set ups. We thank the Institute of Material Sciences (IMS), University of Connecticut for providing us the instruments for analytical experiments.

REFERENCES

[1] Harper WR. Contact and frictional electrification. Oxford: Clarendon P; 1967.

[2] Naik S, Sarkar S, Gupta V, et al. A combined experimental and numerical approach to explore tribocharging of pharmaceutical excipients in a hopper chute assembly. Int J Pharm 2015;49:58–68. doi:10.1016/j.ijpharm.2015.05.081.

[3] Gibson N. Static electricity – an industrial hazard under control? J Electrostat 1997;40:21–30. doi:10.1016/S0304-3886(97)00010-7.
[4] Heibron JL, Finn BS. Electricity in the 17th and 18th centuries: a study of early modern physics. Phys Today 1980;33:46. doi:10.1063/1.2914165.
[5] Hughes JF, Bright AW, Makin B, et al. A study of electrical discharges in a charged water aerosol. J Phys D: Appl Phys 1973;6(8):966–975. doi:10.1088/0022-3727/6/8/309.
[6] Klinkenberg A, van der Minne JL. Klinkenberg A, van der Minne JL, editors. Electrostatics in the petroleum industry. The prevention of explosion hazards. A Royal Dutch-Shell research and development report. Amsterdam: Elsevier Pub. Co.; 1958.
[7] Nifuku M, Ishikawa T, Sasaki T. Static electrification phenomena in pneumatic transportation of coal. J Electrostat 1989;23(C):45–54.
[8] Atallah S. Dust explosions and fires, K. N. Palmer, Chapman and Hall Ltd., London (1973). 396 pages. $18.50. AIChE J 1974;20(2):414. doi:10.1002/aic.690200240.
[9] Mullarney MP, Hancock BC. Improving the prediction of exceptionally poor tableting performance: an investigation into Hiestand's "special case." J Pharm Sci 2004;93(8):2017–2021. doi:10.1002/jps.20108.
[10] Mehrotra A, Muzzio FJ, Shinbrot T. Spontaneous separation of charged grains. Phys Rev Lett 2007;99(5):058001. doi:10.1103/PhysRevLett.99.058001.
[11] Liang S, Zhang J, Fan L. Electrostatic characteristics of hydrated lime powder during transport. Ind Eng Chem Res 1996;35(8):2748–2755. doi:10.1021/ie9506678.
[12] Balachandran W, Machowski W, Gaura E, et al. Control of drug aerosol in human airways using electrostatic forces. J Electrostat 1997;40-1:579–584.
[13] Murtomaa M, Mellin V, Harjunen P, et al. Effect of particle morphology on the triboelectrification in dry powder inhalers. Int J Pharm 2004;282(1):107–114. doi:10.1016/j.ijpharm.2004.06.002.
[14] Cartwright P, Singh S, Bailey AG, et al. Electrostatic charging characteristics of polyethylene powder during pneumatic conveying. IEEE T Ind Appl 1985;IA-21(2):541–546. doi:10.1109/TIA.1985.349702.
[15] Sowinski A, Miller L, Mehrani P. Investigation of electrostatic charge distribution in gas–solid fluidized beds. Chem Eng Sci 2010;65(9):2771–2781. doi:10.1016/j.ces.2010.01.008.
[16] Kulkarni P, Deye GJ, Baron PA. Bipolar diffusion charging characteristics of single-wall carbon nanotube aerosol particles. J Aerosol Sci 2009;40(2):164–179. doi:10.1016/j.jaerosci.2008.09.008.
[17] Forward KM, Lacks DJ, Sankaran RM. Particle-size dependent bipolar charging of Martian regolith simulant. Geophys Res Lett 2009;36(13):L13201. doi:10.1029/2009GL038589.
[18] Crozier WD. Nine years of continuous collection of black, magnetic spherules from the atmosphere. J Geophys Res 1966;71(2):603. doi:10.1029/JZ071i002p00603.
[19] Turner GJ, Stow CD. Quasi-liquid film on ice – evidence from, and implications for contact charging events. Philos Mag A 1984;49(4):L25–L30.
[20] Ette AII, Utah EU. Studies of point-discharge characteristics in the atmosphere. J Atmos Terr Phys 1973;35(10):1799–1809.
[21] Miura T, Koyaguchi T, Tanaka Y. Measurements of electric charge distribution in volcanic plumes at Sakurajima Volcano, Japan. B Volcanol 2002;64(2):75–93. doi:10.1007/s00445-001-0182-1.
[22] Freier GD. The electric field of a large dust devil. J Geophys Res 1960;65(10):3504. doi:10.1029/JZ065i010p03504.
[23] Krauss CE, Horányi M, Robertson S. Experimental evidence for electrostatic discharging of dust near the surface of Mars. New J Phys 2003;5:70. doi:10.1088/1367-2630/5/1/370.
[24] Zheng XJ, Huang N, Zhou Y. Laboratory measurement of electrification of wind-blown sands and simulation of its effect on sand saltation movement. J Geophys Res 2003;108(D10):4322. doi:10.1029/2002JD002572.
[25] Henry PSH. Survey of generation and dissipation of static electricity. Br J Appl Phys 1953;4(2):S6–S11. doi:10.1088/0508-3443/4/S2/302.
[26] Henry PSH. The role of asymmetric rubbing in the generation of static electricity. Br J Appl Phys 1953;4(2):S31–S36. doi:10.1088/0508-3443/4/S2/313.
[27] Diaz A, Fenzel-Alexander D, Wollmann D, et al. Importance of dissociated ions in contact charging. Langmuir 1992;8(11):2698–2706. doi:10.1021/la00047a020.
[28] Davies DK. Charge generation on dielectric surfaces. J Phys D: Appl Phys 1969;2(11):1533–1537. doi:10.1088/0022-3727/2/11/307.
[29] Bard AJ, Liu C. Electrostatic electrochemistry at insulators. Nat Mater 2008;7(6):505–509. doi:10.1038/nmat2160.
[30] Lowell J. The electrification of polymers by metals. J Phys D: Appl Phys 1976;9(11):1571–1585. doi:10.1088/0022-3727/9/11/006.
[31] Otero TF. Electrochemistry electrons create a reaction. Nat Mater 2008;7(6):429–430. doi:10.1038/nmat2188.
[32] McCarty LS, Winkleman A, Whitesides GM. Ionic electrets: electrostatic charging of surfaces by transferring mobile ions upon contact. J Am Chem Soc 2007;129(13):4075–4088. doi:10.1021/ja067301e.
[33] Pence S, Novotny VJ, Diaz AF. Effect of surface moisture on contact charge of polymers containing ions. Langmuir 1994;10(2):592–596. doi:10.1021/la00014a042.
[34] Diaz AF, Wollmann D, Dreblow D. Contact electrification: ion transfer to metals and polymers. Chem Mater 1991;3(6):997–999. doi:10.1021/cm00018a006.
[35] Diaz A. Contact electrification of materials: the chemistry of ions on polymer surfaces. J Adhes 1998;67(1):111–122. doi:10.1080/00218469808011102.
[36] Baytekin HT, Patashinski AZ, Branicki M, et al. The mosaic of surface charge in contact electrification. Science 2011;333(6040):308–312. doi:10.1126/science.1201512.
[37] Law K, Tarnawskyj IW, Salamida D, et al. Investigation of the contact charging mechanism between an organic salt doped polymer surface and polymer-coated metal beads. Chem Mater 1995;7(11):2090–2095. doi:10.1021/cm00059a016.
[38] Lowell J, Truscott WS. Triboelectrification of identical insulators. I. An experimental investigation. J Phys D: Appl Phys 1986;19(7):1273–1280. doi:10.1088/0022-3727/19/7/017.
[39] Lowell J, Truscott WS. Triboelectrification of identical insulators. II. Theory and further experiments. J Phys D: Appl Phys 1986;19(7):1281–1298. doi:10.1088/0022-3727/19/7/018.
[40] Lacks DJ, Duff N, Kumar SK. Nonequilibrium accumulation of surface species and triboelectric charging in single component particulate systems. Phys Rev Lett 2008;100(18):188305. doi:10.1103/PhysRevLett.100.188305.
[41] Murata Y. Photoelectric emission and contact charging of some synthetic high polymers. Jpn J Appl Phys 1979;18(1):1–8.
[42] Zhao H, Castle GSP, Inculet II, et al. Bipolar charging in polydisperse polymer powders in industrial processes. Conf Record 2000 IEEE Industry Appl Conf 35th IAS Ann Meet World Conf Indust Appl Electric Energ (Cat No 00CH37129) 2000;2:835–841. doi:10.1109/IAS.2000.881928.
[43] Li DY, Li W. Variations of work function and corrosion behaviors of deformed copper surfaces. Appl Surf Sci 2005;240(1):388–395. doi:10.1016/j.apsusc.2004.07.017.
[44] Brocks G, Rusu PC. Surface dipoles and work functions of alkylthiolates and fluorinated alkylthiolates on au(111).

J Phys Chem B 2006;110(45):22628–22634. doi:10.1021/jp0642847.
[45] Tomassone MS, Chaudhuri B, Faqih A, et al. DEM simulation for fundamental process understanding. Pharm Technol 2005;29:S28–S35.
[46] Trigwell S, Grable N, Yurteri CU, et al. Effects of surface properties on the tribocharging characteristics of polymer powder as applied to industrial processes. IEEE T Ind Appl 2003;39(1):79–86. doi:10.1109/TIA.2002.807228.
[47] Furthmüller J, Hafner J, Kresse G. Ab initio calculation of the structural and electronic properties of carbon and boron nitride using ultrasoft pseudopotentials. Phys Rev B 1994;50(21):15606–15622. doi:10.1103/PhysRevB.50.15606.
[48] Käckell P, Furthmüller J, Bechstedt F, et al. Characterization of carbon-carbon bonds on the SiC(001)c(2 × 2) surface. Phys Rev B 1996;54(15):10304–10307. doi:10.1103/PhysRevB.54.10304.
[49] Kresse G, Furthmüller J. Efficiency of ab-initio total energy calculations for metals and semiconductors using a plane-wave basis set. Comput Mater Sci 1996;6(1):15–50. doi:10.1016/0927-0256(96)00008-0.
[50] Ernzerhof M, Scuseria GE. Assessment of the Perdew–Burke–Ernzerhof exchange-correlation functional. J Chem Phys 1999;110(11):5029. doi:10.1063/1.478401.
[51] Paier J, Hirschl R, Marsman M, et al. The Perdew-Burke-Ernzerhof exchange-correlation functional applied to the G2-1 test set using a plane-wave basis set. J Chem Phys 2005;122(23):234102. doi:10.1063/1.1926272.
[52] Perdew J, Burke K, Ernzerhof M. Generalized gradient approximation made simple (vol 77, pg 3865, 1996). Phys Rev Lett 1997;78(7):1396. doi:10.1103/PhysRevLett.78.1396.
[53] Zhu Q, Sharma V, Oganov AR, et al. Predicting polymeric crystal structures by evolutionary algorithms. J Chem Phys 2014;141(15):154102. doi:10.1063/1.4897337.
[54] Sarkar S, Cho J, Chaudhuri B. Mechanisms of electrostatic charge reduction of granular media with additives on different surfaces. Chem Eng Process 2012;62:168. doi:10.1016/j.cep.2012.07.009.
[55] Cundall PA, Strack ODL. Discrete numerical model for granular assemblies. Geotechnique 1979;29(1):47–65.
[56] Cundall PA. A computer model for simulating progressive large-scale movements in block rock mechanics. In: Proceedings of the Symposium International Society for Rock Mechanics, vol. 1. Nancy, France; 1971. p. 2–8.
[57] Anand A, Curtis JS, Wassgren CR, et al. Predicting discharge dynamics of wet cohesive particles from a rectangular hopper using the discrete element method (DEM). Chem Eng Sci 2009;64(24):5268–5275. doi:10.1016/j.ces.2009.09.001.
[58] Naik S, Feng Y, Chaudhuri B. Experiment and model-based investigation of comminution in a hammer mill. Int J Comput Meth Exp Measure 2014;2(4):362–373.
[59] Liu PY, Yang RY, Yu AB. DEM study of the transverse mixing of wet particles in rotating drums. Chem Eng Sci 2013;86:99–107. doi:10.1016/j.ces.2012.06.015.
[60] Li H, McDowell GR, Lowndes IS. A laboratory investigation and discrete element modeling of rock flow in a chute. Powder Technol 2012;229:199–205. doi:10.1016/j.powtec.2012.06.032.
[61] McDowell G, Li H, Lowndes I. The importance of particle shape in discrete-element modelling of particle flow in a chute. Geotech Lett 2011;1(3):59–64. doi:10.1680/geolett.11.00025.
[62] Walton OR. Numerical simulation of inclined chute flows of monodisperse, inelastic, frictional spheres. Mech Mater 1993;16(1–2):239–247.
[63] Walton OR, Braun RL. Viscosity, granular-temperature, and stress calculations for shearing assemblies of inelastic, frictional disks. J Rheol (1978–present) 1986;30(5):949–980. http://dx.doi.org/10.1122/1.549893.
[64] Mindlin RD, Deresiewicz H. Elastic spheres in contact under varying oblique forces. J Appl Mech 1953;20:327–344.
[65] Bueche F. Introduction to physics for scientists and engineers. Am J Phys 1970;38(2):274. doi:10.1119/1.1976308.
[66] Lowell J, Rose-Innes AC. Contact electrification. Adv Phys 1980;29(6):947–1023.
[67] Matsusaka S, Ghadiri M, Masuda H. Electrification of an elastic sphere by repeated impacts on a metal plate. J Phys D: Appl Phys 2000;33(18):2311–2319. doi:10.1088/0022-3727/33/18/316.
[68] Watanabe H, Ghadiri M, Matsuyama T, et al. Triboelectrification of pharmaceutical powders by particle impact. Int J Pharm 2007;334(1):149–155. doi:10.1016/j.ijpharm.2006.11.005.
[69] Hogue MD, Calle CI, Weitzman PS, et al. Calculating the trajectories of triboelectrically charged particles using discrete element modeling (DEM). J Electrostat 2008;66(1):32–38. doi:10.1016/j.elstat.2007.08.007.
[70] Wang Y, Liu X, Burton J, et al. Ferroelectric instability under screened coulomb interactions. Phys Rev Lett 2012;109(24):247601.
[71] Ali SF, Inculet II, Tedoldi A. Charging of polymer powder inside a metallic fluidized bed. J Electrostat 1999;45(3):199–211. doi:10.1016/S0304-3886(98)00050-3.
[72] Williams MW. Triboelectric charging of insulators – evidence for electrons versus ions. IEEE T Ind Appl 2011;47(3):1093–1099. doi:10.1109/TIA.2011.2126032.